Title

Motion-free volumetric retinal imaging with adaptive optics spectral-domain optical coherence tomography

ISBN

9780819461810

Authors

Zhang, Yan
Rha, Jungtae
Cense, Abraham
et al.

Publication Date

2006-02-09

DOI

10.1117/12.649006

Peer reviewed

Motion-free volumetric retinal imaging with adaptive optics spectral-domain optical coherence tomography

Yan Zhang[1], Jungtae Rha[1], Abraham Cense[1], Ravi S. Jonnal[1], Weihua Gao[1],
Robert J. Zawadzki[2], John S. Werner[2],
Steve Jones[3], Scot Olivier[3], and
Donald T. Miller[1]
[1]School of Optometry, Indiana University, Bloomington, IN 47405
[2]Department of Ophthalmology and Vision Science, University of California Davis, Sacramento, CA 95817
[3]Lawrence Livermore National Laboratory, 700 East Avenue, Livermore, CA 74550

Abstract

We report first observations of the three-dimensional morphology of cone photoreceptors in the living human retina. Images were acquired with a high-speed adaptive optics (AO) spectral domain optical coherence tomography (SD-OCT) camera. The AO system consists of a Shack-Hartmann wavefront sensor and bimorph deformable mirror (AOptix) that measure and correct the ocular and system aberrations at a closed-loop rate of 12 Hz. Unlike previous AO-OCT and AO-SLO instruments, the bimorph mirror was strategically positioned between the XY mechanical scanners and the subject's eye so as to avoid beam distortion at the pupil plane, which is created when the mirror compensates for the refractive error of the eye. This new configuration is evaluated empirically and with commercial ray tracing software. The SD-OCT system consists of a superluminescent diode and a 512 pixel line scan charge-coupled device (CCD) that acquires 75,000 A-scans/sec. This rate is more than two times faster than that previously reported. Retina motion artifiacts were minimized by quickly acquiring small volume images of the retina with and without AO compensation. Camera sensitivity was sufficient to detect reflections from all major retinal layers. The distribution of bright spots observed within C-scans at the inner segment / outer segment (IS/OS) junction and at the posterior tips of the OS were found to be highly correlated with one another and with the expected cone spacing. No correlation was found between the IS/OS junction and either the plexiform layers or the layers immediately behind the OS posterior tips.

Keywords: Adaptive optics, spectroscopy, optical coherence tomography, eye, retina, photoreceptors

1. Introduction

SD-OCT is a non-invasive, interferometric imaging modality that provides very high speed, sensitivity and axial resolution, which are attractive for non-invasive imaging of the retina [1,2]. The transverse resolution of SD-OCT in the eye, however, is poor - being no better than 15 μm - due to a small imaging pupil (<2mm) and the presence of ocular aberrations. Fundus cameras and scanning laser ophthalmoscopes equipped with AO, on the other hand, have demonstrated substantially higher lateral resolution approaching 2 μm [3-6]. However, these cameras exhibit noticeably poorer axial resolution due to the low numerical aperture (NA) of the eye (even when dilated) and are unable to create volume images of the retina with a 3D resolution that is comparable to the size of individual cells.

Given the complementary resolution advantages of AO and SD-OCT, their combination should yield a resolution approaching a few microns in all three dimensions. To date, AO has been combined with free space parallel SD-OCT [6] and fiber based SD-OCT [7,8]. While these instruments have been reported to achieve lateral and axial resolutions up to 3 μm and 2-3 μm in the eye, respectively, all have noticeable limitations for volumetric imaging of single cells. The AO free space SD-OCT acquired B-scans that showed individual cone photoreceptors resolved in both axial and lateral dimensions. However, the instrument was not designed for volume imaging as it had no mechanism to laterally scan the line illumination and detector across the retina. The AO fiber based SD-OCT on the other hand acquired volume images whose B-scans revealed cone photoreceptors. However, the long exposure durations (<6 s for a volume image), the saw-tooth scan pattern, and the large scanning range (1.67x0.67 deg) exposed the volume images to substantial retina motion artifacts that hampered observation of cone photoreceptors in extracted C-scans.

Ophthalmic Technologies XVI, edited by Fabrice Manns, Per G. Söderberg, Arthur Ho,
Proc. of SPIE Vol. 6138, 613802, (2006) · 1605-7422/06/$15 · doi: 10.1117/12.649006

To address these limitations, we have developed an AO fiber based SD-OCT retina camera that acquires A-scans faster (75,000 per sec), raster scans over a shorter distance (37 A-scans per B-scan), and employs a triangular scan pattern that further reduces the time delay between consecutive B-scans. Collectively, these permit small rectangular retinal patches to be imaged at a volume rate of 19 B-scans per 10 msec, a time duration that is short enough to freeze the motion of the retina in a fixating eye. In this paper we find that the 3D resolution, sensitivity, and volume rate of this camera is sufficient for imaging the cone mosaic in the living human retina. We measure the sensitivity of the AO SD-OCT camera, quantify changes in the retinal reflectance caused by compensation of ocular aberrations, and compare C-scan images at different depths in the retina.

2. Description of the AO SD-OCT camera

The camera consists of three channels: (1) sample channel for collecting the reflected light from an eye, (2) reference channel whose optical path length matches that in the sample channel, and (3) detection channel for capturing retinal images. Figure 1 shows a detailed layout of the camera.

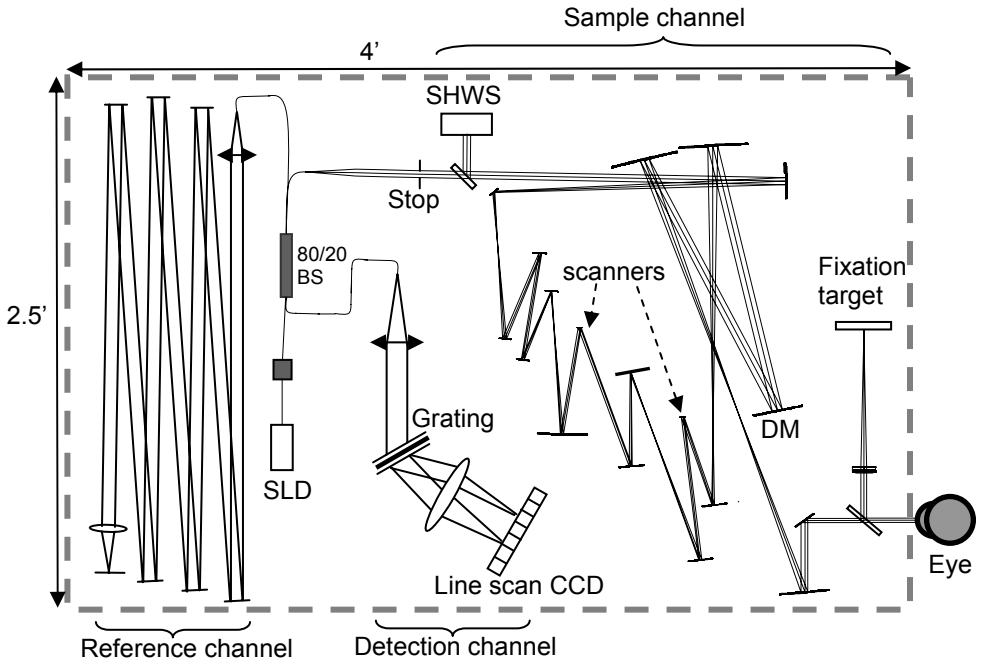

Figure 1. Layout of the AO SD-OCT retina camera. The camera consists of three channels: (1) sample channel, (2) reference channel, and (3) detection channel. The AO system is integrated into the sample channel.

A 10 mW broadband superluminescent diode (SLD) (λ= 842 nm, $\Delta\lambda$= 50 nm) is used to illuminate the retina. In the sample channel, light exiting the fiber propagates through five relay telescopes consisting of ten spherical mirrors with protected silver coating. The pupil of the eye is conjugate to the AOptix mirror, the two scanning mirrors, the 20×20 lenslet array (f=30mm, lenslet dia.=500μm) of the SHWS, and a circular aperture positioned immediately after the collimation optic for the SLD. The AO system is incorporated into the sample channel and is designed to operate simultaneously with the SD-OCT. A 90/10 pellicle is inserted after the system stop to redirect 10% of the light reflected from the eye to the SHWS. The lenslet array samples the wavefront across a 6.6 mm pupil of eye. The array of focal spots produced by this lenslet array was recorded with a Dalsa 1M60 CCD camera. Displacements of the spots compared to a preset reference are fed into a direct slope control algorithm to be rapidly converted to control voltages for the AOptix mirror. The AO can operate up to 30 wavefront measurements and corrections per second, although the typical rate during the experiment was 12 Hz due to signal to noise (S/N) requirement of SHWS. The AOptix bimorph contains 37 actuators and has a maximum displacement of 32 μm.

The large stroke is highly attractive for retinal imaging as it permits compensation of relatively large amounts of sphere and cylindrical refractive error, thereby obviating the need for trial lenses. However such relatively large corrections present challenges for the system design. For example, our performance analysis with commercial ray tracing software (Zemax, Inc.) revealed that mirror correction of defocus (sphere) and astigmatism (cylinder) can generate noticeable beam distortion at the pupil of the eye for our original AO-OCT layout in which the bimorph mirror is placed between the SLD light source and XY scanners. This arrangement is similar to that previously reported [7,8]. The distortion increases with the magnitude of the mirror correction (or equivalently refractive error of the subject) and the reflection angle at the spherical mirrors in the relay telescopes. Beam distortion at the pupil reduces resolution in one dimension and causes vignetting in the other one. To illustrate, Figure 2 shows the outcome of a Zemax ray trace simulation for our original AO-OCT design. Shown is the beam shape at the pupil when the radius of curvature of the AOptix mirror is set to compensate 0 and ±3D of defocus. Note that for the ±3D cases, the beam shape is oval with the short axis roughly half that of the other axis. For the 0 D case, the beam is approximately circular. To overcome this difficulty and regain effective use of the full mirror stroke, we discovered that strategic placement of the AOptix mirror very close to the eye, i.e., one relay telescope away from the eye, yielded essentially no beam distortion. This arrangement is effective because it minimizes the propagation of ocular refractive errors through the system prior to compensation.

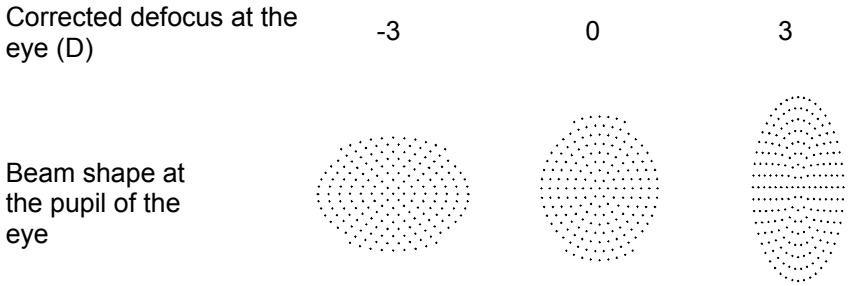

Figure 2. Beam shape at the pupil of the eye when 3D defocus aberration is corrected by the DM. Beam diameter for 0 D case (middle) is 6.6 mm.

In the reference channel, light is collimated by a microscope objective lens (10X) and propagates between six planar mirrors with protected silver coating. The reference beam is then focused onto the 7th planar mirror by a thin singlet plano-convex lens and reflected back to the fiber. A water vial is placed in the beam path to compensate dispersion induced by the eye. The overall optical path length is set to match that of the sample channel (4.7m).

Light from the sample and reference channels are combined using an 80/20 fiber coupler. Light exiting the fiber coupler is collimated by an achromat doublet lens (f=75mm) and diffracted by a 1,200 lines/mm transmission grating (Wasatch Photonics) at Littrow's angle. Grating efficiency for the first order is 86% at 830 nm. A multi-element photographic lens focuses light on a line-scan CCD detector (12 bit, 512 pixels Atmel). Custom software was developed to acquire raw spectral images, subtract reference spectra, interpolate into *k*-space, balance dispersion, Fourier transform, and finally display the reconstructed volumetric retinal images. Exposure level at the cornea was 0.43 mW and complies with the American National Standards Institute (ANSI) [9].

3. Methods and Results

3.1 Protocol for motion free retinal imaging

Small patches of retina (285 μm × 37 μm) in one subject were imaged within a time duration of 150 ms. While retina motion artifacts such as image distortion will be present across the entire volume image, small 19 μm × 37 μm sub-sections of the volume image will be essentially free of motion artifacts as these are acquired with 10 ms. The slow scan employed a saw-toothed pattern that cycled at 6.7 Hz; the fast scan used a symmetric triangular pattern that cycled at 1.0 KHz. Images were collected using the following protocol: (1) administer one drop of 1% Tropicamide, (2) align subject's eye to the AO-OCT instrument using a dental impression attached to a sturdy XYZ translation stage, (3) collect small volume retinal images with and without AO correction, (4) repeat step 3 for several retinal locations.

3.2 OCT sensitivity experiment

Prior to retinal imaging, the sensitivity of the spectral OCT system was measured by substituting a model eye in the sample channel. A neutral density filter was placed in the reference channel and limited the reference beam intensity to one quarter (49,485 electrons) of the CCD pixel capacity (197,940 electrons). One thousand CCD frames of the reference beam were captured and averaged. Then, interference spectra were recorded as the optical path length of the reference channel was incremented in 200 μm steps via a one dimensional stage. Measurements were acquired across a 1.2 mm range that is equivalent to 0.87 mm in retinal tissue (assuming n_{retina} = 1.38). For each step, B-scans were reconstructed and used to determine the experimental sensitivity. To calculate theoretical sensitivity, optical power of the light reflected from model eye was also measured at the fiber coupler's input end of the detection channel by a power meter (Newport, Inc.). The power incident on the model eye was 430 μW, integration time of the CCD line scan was 20 μs, and the detection channel efficiency was measured at 21%.

Figure 3 shows measured sensitivity as a function of depth. Sensitivity peaks at 91 dB, which is in good agreement with the theoretical value of 95 dB. The figure also shows an 8 dB/mm sensitivity drop, due to limitations of the detection channel, in particular, the under sampling of interference fringes at high frequency. Imaging depth in air is 1.5 mm equivalent to 1.1 mm in tissue. The theoretical full width at half height (FWHH) axial resolution (= $2\ln 2/\pi * \lambda_o^2/\Delta\lambda n_{retina}$) in retinal tissue for the 842 nm SLD is 4.7 μm.

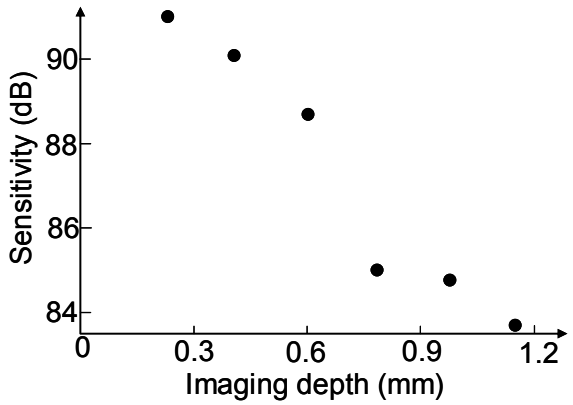

Figure 3. OCT sensitivity as a function of depth in air.

3.3 AO performance:

Figure 4 (a) shows the measured wave aberrations across the subject's 6.6 mm pupil before and after AO correction. AO compensation clearly reduces the magnitude of the aberrations and increases the Strehl ratio from 7% to 35%. Figure 4(b) shows a root mean square (RMS) trace of the measured wave aberrations for the same subject before and during AO dynamic correction. Once initiated, full correction is achieved in a few iterations of the AO loop and typically reaches a mean corrected RMS of about 0.12 μm. The results presented in Fig. 4 are typical for this subject.

3.4 AO-OCT volume images

Using as representative examples the AO-OCT volume images collected on the subject at 2° retinal ecc., Fig. 5 illustrates the two main benefits of AO for OCT retinal imaging. These benefits are increased S/N and increased transverse resolution. Figure 5(a) shows two extracted C-scans of the IS/OS junction, acquired with and without AO. In order to visualize differences in S/N between the two conditions, both C-scans were mapped to the same gray scale, i.e., normalized to the brightest pixel from either C-scan. With this mapping, it is visually obvious that the C-scan acquired with AO is much brighter than the one acquired without. Quantitative analysis of the C-scans confirms that the S/N increased by 10 dB. Figure 5(b) shows the same two C-scans, but with each mapped to their own gray scale so as to permit better visualization of the retinal structure in either image. A regular array of individual bright spots, which likely correspond to reflected light guided by individual cone photoreceptor cells, is readily evident in the C-scan image acquired with AO. No such regular pattern is visible in the image acquired without AO. This latter image does contain high frequency irregular structure, but the random nature of the pattern and size suggests this is primarily speckle superimposed on the retinal signature. In general, correction of the ocular aberrations with AO improves image quality and permits the observation of individual cone photoreceptor cells.

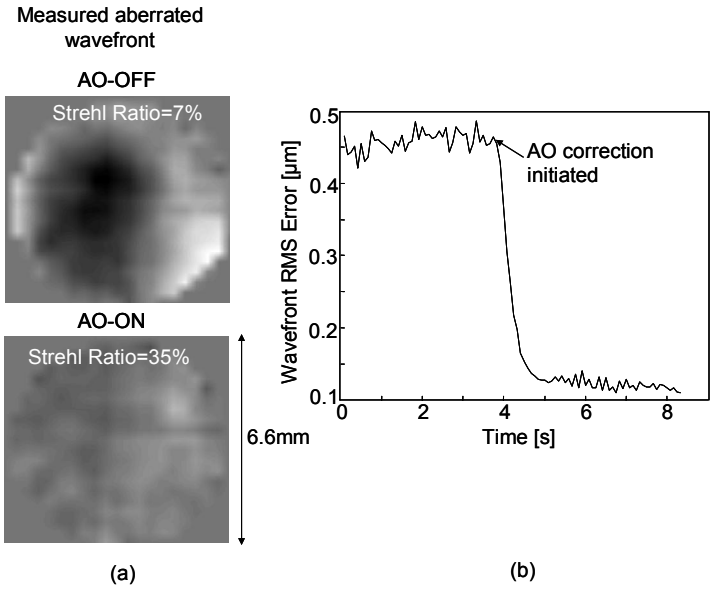

Figure 4 (a) Residual wave aberrations across a 6.6 mm pupil in one subject as measured by the SHWS before and after AO compensation. (b) An RMS trace of the residual wave aberrations is shown for one subject before and during AO dynamic correction.

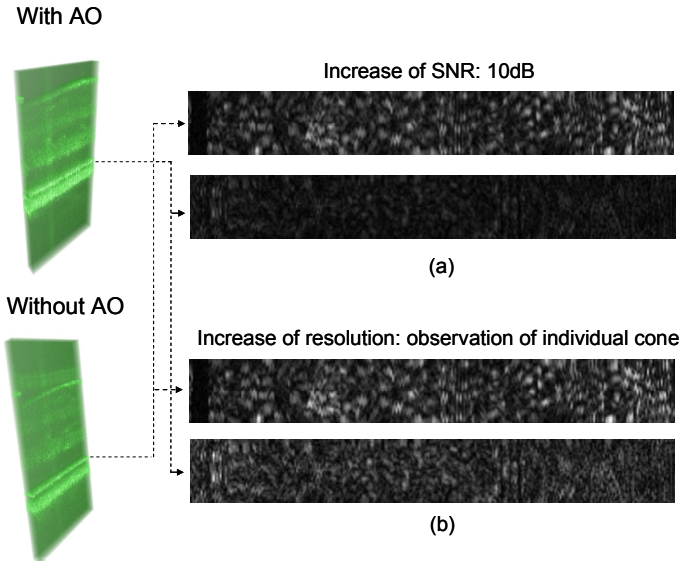

Figure 5 (a) C-scan images at the junction between the inner and outer segments (IS/OS) are shown with and without AO. The two images are normalized to the same gray scale. (b) The same C-scan images are shown again, but with each mapped to their own gray scale so as to permit better visualization of the retinal structure. Both volume images were acquired at essentially the same 2^{o} retinal eccentricity.

As further analysis of the volume images, C-scans were extracted from the outer plexiform layer (OPL), IS/OS junction, posterior tip of the OS, and retinal pigmented epithelium (RPE). The four C-scans are shown in Fig. 6. The OPL and RPE images appear dominated by high frequency irregular structure that is suggestive of speckle. The other two images have a markedly different appearance with a more or less regular array of bright spots that reasonably matches the spacing of cone photoreceptors for this retinal eccentricity. Of significant interest, the bright spot pattern (cone mosaic) at the IS/OS junction and the posterior tip of the OS appear to have similar features. Cross correlation of these two

images (see Fig. 7) does indeed reveal a strong correlation. This suggests both reflections are waveguided by the photoreceptor optics and further strengthens the common belief that the photoreceptor outer segment acts as a fiber-like structure. Interestingly this strong correlation was found only between these two layers. This latter finding is supportive evidence that the waveguided light that reflects back out of cone photoreceptors (as routinely observed with AO fundus cameras and AO scanning laser ophthalmoscopes) originates from only two thin layers. We found no evidence that the light reflected back from the RPE was recaptured by the overlying photoreceptors.

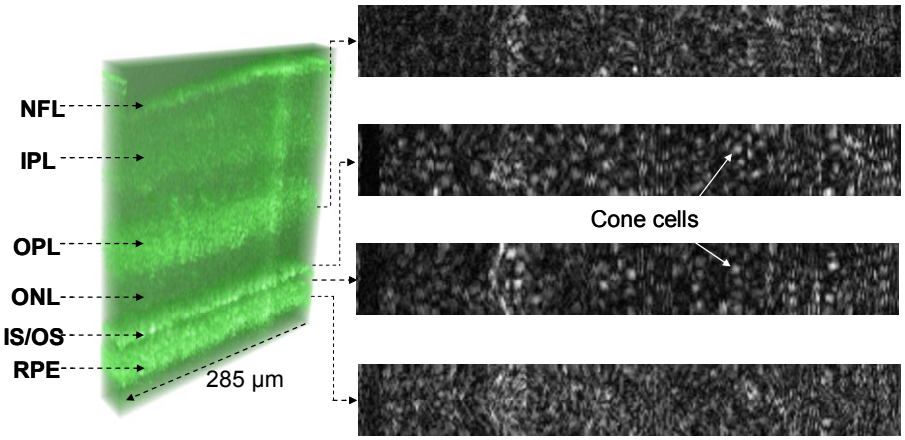

Figure 6 C-scan images extracted from different depths in the volume AO-OCT image. C-scans correspond to the OPL, IS/OS junction, posterior of OS, and RPE.

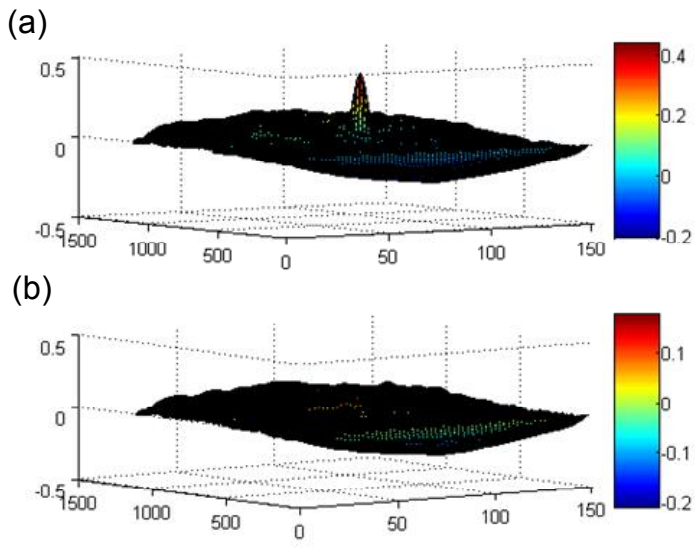

Figure 7 (a) Cross correlation between C-scans at the IS/OS junction and (a) posterior tip of OS and (b) RPE.

4. Conclusion

We demonstrate a fiber based AO spectral-domain OCT camera for imaging living retina at high 3D resolution (3x3x4.7 μm) and speed (75,000 A-scan/sec). This acquisition rate is more than two times faster than that previously reported in the literature. Unlike previous AO-OCT and AO-SLO instruments, the bimorph mirror was strategically positioned between the XY mechanical scanners and the subject's eye so as to avoid beam distortion at the pupil plane, which was predicted for our original AO SD-OCT system design. Retina motion artifacts were minimized by quickly acquiring

small volume images of the retina with and without AO compensation. Initial results demonstrate a ~10 dB increase in S/N of the photoreceptor layer with AO correction. Camera sensitivity was sufficient to detect reflections from all major retinal layers. The distribution of bright spots observed within C-scans at the IS/OS junction and at the posterior tips of the OS were found highly correlated to each other (confirmed by cross correlation) and to the expected cone spacing. No correlation was found between the IS/OS junction and the plexiform layers as well as immediately behind the OS posterior tips. In general, AO spectral-OCT represents a potentially powerful tool for non-invasively imaging the retina at the single cell level.

Acknowledgement

Financial support was provided by the National Eye Institute grant 5R01 EY014743. This work was also supported in part by the National Science Foundation Science and Technology Center for Adaptive Optics, managed by the University of California at Santa Cruz under cooperative agreement No. AST-9876783.

References

1. D. Huang, E.A. Swanson,, C.P. Lin, J.S. Schuman, W.G. Stinson, W. Chang, M.R. Hee, T. Flotte, K. Gregory, C. Puliafito, J.G. Fujimoto, "Optical Coherence Tomography", Science **254**, 1178-81, (1991)
2. Cense B, Nassif N, Chen T, Pierce M, Yun S, Park B, Bouma B, Tearney G, de Boer J., "Ultrahigh-resolution high-speed retinal imaging using spectral-domain optical coherence tomography", Optics Express 2004; 12(11): 2435-2447.
3. Liang J, Williams D, Miller D., "Supernormal vision and high-resolution retinal imaging through adaptive optics", Journal of Optical Society of America A. 1997; 11: 2884-2892.
4. A. Roorda, F. Romero-Borja, W. J. Donnelly, H. Queener, T. J. Hebert, and M. C. W. Campbell, "Adaptive optics scanning laser ophthalmoscopy," Optics Express 10, 405-412 (2002). http://www.opticsexpress.org/abstract.cfm?URI=OPEX-10-9-405.
5. N. Doble, G. Yoon, L. Chen, P. Bierden, B. Singer, S. Olivier, and D. R. Williams, "Use of a microelectromechanical mirror for adaptive optics in the human eye," Opt. Lett. 27, 1537-1539 (2002).
6. Y. Zhang, J. Rha, R. S. Jonnal, and D. T. Miller, "Adaptive optics parallel spectral domain optical coherence tomography for imaging the living retina," Optics Express Vol. 13, No. 12, 4792-4811 (2005).
7. R. J. Zawadzki, S. M. Jones, S. S. Olivier, M. Zhao, B. A. Bower, J. A. Izatt, S. Choi, S. Laut, and J. S. Werner, "Adaptive-optics optical coherence tomography for high-resolution and high-speed 3D retinal in vivo imaging," Optics Express Vol. 13, No. 21, 8532-8546 (2005).
8. E. J. Fernández, B. Považay, B. Hermann, A. Unterhuber, H. Sattmann, P. M. Prieto, R. Leitgeb, P. Ahnelt, P. Artal and W. Drexler, "Three-dimensional adaptive optics ultrahigh-resolution optical coherence tomography using a liquid crystal spatial light modulator," Vision Research Vol. 45, 3432-3444 (2005).
9. American National Standard for the Safe Use of Lasers ANSI Z136.1. (Laser Institute of America, Orlando, FL, 2000).